NUMERICAL STUDY ON NECKING-TYPE BIFURCATIONS IN VOID-CONTAINING ELASTIC-PLASTIC MATERIAL

M. KLEIBER

Institute of Fundamental Technological Research, Polish Academy of Sciences, Warsaw, Poland

Abstract—The axisymmetric necking in a circular cylindrical specimen under uniaxial tension is analysed. The "finite strain" elastic–plastic constitutive models employed in this study encompass the classical J_2-flow theory and a non-associated flow theory of Gurson which approximately describes ductile fracture on the microscale. For the former theory the comparison solid of Hill is additionally considered while the comparison solids recently introduced by Raniecki are thoroughly analysed regarding the latter theory. The imperfection-type approach is used via the direction integration of the finite element equations of equilibrium. The location of the primary bifurcation point on the equilibrium path and the accuracy of its estimation by means of the "comparison solid" approach are discussed. The attention is focused on the bar with shear-free ends but the results for the bar with ends cemented to rigid grips are also given.

1. INTRODUCTION

Plastic instability is a failure mechanism that is frequently observed in bodies under tensile loading and in columns, plates and shells under compression. A great number of papers has been written on this subject for both its practical importance and mathematical elegance. Generally, two groups of methods exist for the analysis of instability phenomena which can be classified as a bifurcational approach and a direct integration approach, respectively. Under the idealized loading conditions, specimen geometry and material homogeneity instability of the primary mode of deformation is usually associated with bifurcation from the fundamental equilibrium path to a secondary equilibrium path. The Hill's theory of uniqueness and stability in elastic–plastic solids provides an effective analytical tool to deal with such situations. Many publications can be cited with reference to problems posed in this way [1–8].

Unavoidable deviations from the perfect conditions often result in significant reductions of the critical loads or strains, at which failure occurs. Therefore, it is important to know how sensitive is the structure to different imperfection patterns [9–11].

Imperfect structural problems form simultaneously a starting point for the direct integration approach to the instability analysis. According to this concept the nonlinear differential equations describing the behaviour of the imperfect structures are integrated in a step-by-step manner leading to the overall force–displacement characteristics of the structure with some singular points signalling the possible loss of stability. This method is costly and requires repetitive computations for different imperfections, supplies however a very detailed information on the structural behaviour [12–16]. In particular, for problems with non-uniform pre-critical response and for those requiring post-critical behaviour evaluation the direct methods still seem to be superior to the bifurcational methods as the latter have so far been effectively used in analysing some model structural configurations only and not in dealing with real complex structures of engineering importance.

The Hill's theory of bifurcation and uniqueness applies to a class of elastic–plastic materials the most useful of which seems to be at present the so-called finite strain version of the J_2-flow theory model. It is the model based upon the conventional plastic flow rule (normality rule) associated with a smooth yield surface of von Mises kind and with the finite deformation effects accounted for by including some convective terms in the definition of the stress rate [7, 17]. It was proved by Hill[1] that a "no unloading" comparison solid can be used (applying a quadratic functional for testing for bifurcation) to yield a lower bound to the primary bifurcation load for the genuine elastic–plastic solid described by the J_2-flow theory and the bifurcations are identical in many cases. This is an important result (provided the estimate so obtained is close enough to the real bifurcation point) as the effective inclusion of the local unloading from the

plastic flow can sometimes lead to serious difficulties in developing analytical or numerical methods of plastic analysis.

The J_2-flow theory has found a widespread interest in application to different engineering problems concerning uniqueness and stability such as necking in bars and sheets, bulging in shells and buckling of columns. However, there exists at present some experimental evidence that some void-containing metals (as well as some soil- and rock-like materials) do not obey the normality rule. The elastic–plastic behaviour of such materials is expected to be better described by non-associated plastic flow laws which have been first discussed in [18].

Microscopic voids in ductile materials may play a crucial role in various problems of inelastic instability. An approximate continuum representation of the response of a ductile void-containing material can be obtained by accounting for the plastic dilatancy that will be the apparent macroscopic effect of void growth. The inclusion of plastic dilatancy and of pressure sensitivity of yield into elastic–plastic constitutive equations leads to a form of the general relations describing non-associated plasticity. Of particular interest here is the approximate constitutive theory developed by Gurson [19, 20] who specified the equations in detail on the basis of some rigid-plastic computations for spherical void geometries. The theory of Gurson has already been used in a number of investigations on various fracture mechanisms[21-25]. Here we are to use this theory in analysing the axisymmetric necking problem. However, the necking mechanism is investigated by considering an elastic–plastic specimen containing a non-uniform distribution of microscopic voids rather than having a shape imperfection. Further, the nature of the necking-type bifurcation is studied by using some "comparison solids" introduced recently in [26].

All the computations are carried out by means of the finite element method which is used for the direct integration of the equations describing an imperfect axisymmetric specimen. To this aim a special numerical procedure based upon the Newton–Raphson iteration scheme has been developed as shortly described in Section 3. The paper closes with a detailed presentation of the numerical results obtained for two sets of boundary conditions modelling the specimen ends as either cemented to rigid grips or shear free.

2. CONSTITUTIVE RELATIONSHIP

The J_2-finite strain flow theory as well as its generalization proposed in [19, 20] for the description of void-containing metals are shortly reviewed below. The formulation has a form particularly suitable to the updated Lagrangian approach. Our analysis is restricted to the analysis of inelastic deformation processes for which the elastic part of strain is derivable from the generalized Hooke's law. This implicitly means that elastic strains are infinitesimal.

The three-dimensional form of the equations is presented only as its specialization to an axisymmetric problem is straightforward and in the case of a voided material follows the lines sketched in[24]. For the sake of simplicity all the quantities below are referred to a cartesian coordinate system fixed at the beginning of the current step.

The fundamental postulates we start with are the summability of the elastic $d_{ij}^{(e)}$ and plastic $d_{ij}^{(p)}$ parts of the strain rate and the flow rule

$$d_{ij} = \frac{1}{\zeta} s_{ij} (s_{kl} \dot{\sigma}_{kl}) \tag{2.1}$$

associated with von Mises yield condition

$$\phi = \frac{3}{2} \frac{\sigma_{ij}^S \sigma_{ij}^D}{\bar{\sigma}^2} - 1 = 0 \tag{2.2}$$

where $\dot{\sigma}_{ij}$ = rate of the second Piola–Kirchhoff stress tensor defined on the current (beginning of the step) configuration; s_{ij} = normal to the yield surface defined as

$$s_{ij} = \frac{3}{2} \frac{\sigma_{ij}^D}{\bar{\sigma}}, \ s_{ij} s_{ij} = \frac{3}{2}, \tag{2.3}$$

σ_{ij}^D = deviator of the Cauchy stress tensor σ_{ij}, $\sigma_{ij} = \bar{\sigma}_{ij}$ at the beginning of the step,

$$\bar{\sigma} = \left(\frac{3}{2}\sigma_{ij}^D\,\sigma_{ij}^D\right)^{1/2}, \tag{2.4}$$

$$\zeta = \frac{E\,E_T}{E - E_T}, \tag{2.5}$$

E = Young modulus; E_T = slope of the true stress–natural strain curve at stress level $\bar{\sigma}$. The J_2-flow theory generalized to finite strains is characterized by the following rate-type constitutive equation

$$\dot{\sigma}_{ij} = L_{ijkl}\,d_{kl}, \quad L_{ijkl} = L_{klij}, \quad L_{ijkl} = L_{ijlk} \tag{2.6}$$

in which d_{ij} = symmetric part of the velocity gradient,

$$L_{ijkl} = L_{ijkl}^{(e)} - \alpha\,\frac{\bar{s}_{ij}\,\bar{s}_{kl}}{\zeta^*} - \frac{1}{2}(\sigma_{ik}\delta_{jl} + \sigma_{jk}\delta_{il} + \sigma_{il}\delta_{jk} + \sigma_{jl}\delta_{ik})$$

$$= \frac{E}{1+\nu}\left[\frac{\nu}{1-2\nu}\delta_{ij}\,\delta_{kl} + \frac{1}{2}(\delta_{ik}\,\delta_{jl} + \delta_{il}\delta_{jk}) - \alpha\,\frac{\sigma_{ij}^S\,\sigma_{kl}^D}{\bar{\omega}}\right] - \frac{1}{2}(\sigma_{ik}\,\delta_{jl} + \sigma_{jk}\,\delta_{il} + \sigma_{il}\,\delta_{jk} + \sigma_{jl}\,\delta_{ik})$$

$$= \left[\left(k - \frac{2}{3}G\right)\delta_{ij}\,\delta_{kl} + G(\delta_{ik}\,\delta_{jl} + \delta_{il}\,\delta_{jk}) - \alpha\,\frac{G\,\dfrac{\sqrt{3}\,\sigma_{ij}^D}{\bar{\sigma}} \cdot G\,\dfrac{\sqrt{3}\,\sigma_{kl}^D}{\bar{\sigma}}}{\dfrac{1}{3}\zeta + G} - \frac{1}{2}(\sigma_{ik}\delta_{jl} + \sigma_{jk}\delta_{il} + \sigma_{il}\delta_{jk} + \sigma_{jl}\delta_{ik}),\right. \tag{2.7}$$

$$L_{ijkl}^{(e)} = \frac{E}{1+\nu}\left[\frac{\nu}{1-2\nu}\delta_{ij}\,\delta_{kl} + \frac{1}{2}(\delta_{ik}\,\delta_{jl} + \delta_{il}\,\delta_{jk})\right], \tag{2.8}$$

$$\bar{\omega} = \frac{2}{3}\bar{\sigma}^2\,\frac{\dfrac{E}{E_T} - \dfrac{1-2\nu}{3}}{\dfrac{E}{E_T} - 1} = \frac{2}{3}\bar{\sigma}^2\left(1 + \frac{\zeta}{3G}\right) = \frac{2\bar{\sigma}^2}{9G}\,\zeta^*, \tag{2.9}$$

$$\bar{s}_{ij} = L_{ijkl}^{(e)}\,s_{kl} = \frac{E}{1+\nu}\,s_{ij} = G\,\frac{3\sigma_{ij}^D}{\bar{\sigma}}, \tag{2.10}$$

$$\alpha = \begin{cases} 1, & \text{for } \bar{\sigma} = \bar{\sigma}_{\max} \text{ and } \dot{\bar{\sigma}} \geq 0, \\ 0, & \text{for } \bar{\sigma} < \bar{\sigma}_{\max} \text{ or } \dot{\bar{\sigma}} < 0, \end{cases} \tag{2.11}$$

ν = Poisson ratio,
K = bulk modulus,
G = elastic shear modulus,

$$\zeta^* = \zeta + \bar{s}_{ij}\,s_{ij} = \zeta + 3G. \tag{2.12}$$

It can be seen from eqns (2.6) and (2.7) [25], that the plastic strain rate can also be written as

$$d_{ij}^{(p)} = s_{ij}\,\frac{s_{kl}L_{klmn}^{(e)}d_{mn}}{\zeta + s_{kl}L_{klmn}^{(e)}s_{mn}} = s_{ij}\,\frac{s_{kl}\dot{\sigma}_{kl}^*}{\zeta + 3G} = s_{ij}\,\frac{s_{kl}\dot{\sigma}_{kl}^*}{\zeta^*} \tag{2.13}$$

with the fictitious "elastic" stress rate $\dot{\sigma}_{ij}^*$ defined as

$$\dot{\sigma}_{ij}^* = L_{ijkl}^{(e)}\,d_{kl}. \tag{2.14}$$

Both the plastic strain rate definitions given by eqns (2.1) and (2.13) are of fundamental significance in developing effective finite element algorithms for solving boundary-value problems; this will be further commented upon in Section 3.

The J_2-flow theory of plasticity has been recently generalized in [19, 20, 22] with the intention to model process of ductile void growth in metals. The model does in fact belong to a broader class of inelastic materials showing the effects of plastic dilatancy and flow non-normality.

The approximate yield condition derived by Gurson [19, 20], based on a rigid-perfectly plastic upper bound solution for spherically symmetric deformations around a single spherical void, is of the form

$$\phi = \frac{3}{2} \frac{\sigma_{ij}^D \sigma_{ij}^D}{\sigma_M^2} + 2f \cosh\left(\frac{\sigma_{kk}}{2\sigma_M}\right) - (1 + f^2) = 0, \tag{2.15}$$

in which σ_{ij} is the macroscopic stress tensor, while f is the current void volume fraction. The actual microscopic state of stress in the matrix material is represented by the equivalent tensile flow stress σ_M. The matrix material is taken to be plastically incompressible. Following Needlemen and Rice [22], the rate of the current void volume fraction is given by the expression

$$\dot{f} = (1 - f)\, d_{kk}^{(p)} + \frac{\hat{K}}{\sigma_M}\left(\dot{\sigma}_M + \frac{\dot{\sigma}_{kk}}{3}\right) \tag{2.16}$$

where the first term describes the void growth while the other ones are responsible for the stress controlled nucleation of voids. Here the void nucleation rate is represented in terms of the parameter $\hat{K}$ which is the volume fraction of particles converted to voids per unit fractional increase in stress. It has been suggested in [22] to take $\hat{K}$ of the order 0.01–0.1 for steel.

A number of further assumptions discussed in [22–25], for instances, leads to the plastic flow rule of the form

$$d_{ij}^{(p)} = \frac{1}{H} \frac{\partial \phi}{\partial \sigma_{ij}}\left(\frac{\partial \phi}{\partial \sigma_{kl}} + \frac{\partial \phi}{\partial f} \frac{\hat{K}}{3\sigma_M}\delta_{kl}\right)\dot{\sigma} \tag{2.17}$$

where

$$H = -\left[\frac{\partial \phi}{\partial f}(1 - f)\delta_{ij} + \left(\frac{\partial \phi}{\partial f}\frac{\hat{K}}{\sigma_M} + \frac{\partial \phi}{\partial \sigma_M}\right)\zeta \frac{\sigma_{ij}}{(1 - f)\sigma_M}\right]\frac{\partial \phi}{\partial \sigma_{ij}}. \tag{2.18}$$

The general non-associated plastic flow rule has usually been discussed [18, 26], in the form

$$d_{ij}^{(p)} = \frac{1}{\zeta} s_{ij}^1 (s_{kl}^2 \dot{\sigma}_{kl}) \tag{2.19}$$

in which

$$s_{ij}^1 = \frac{3}{2}\frac{\sigma_{ij}^D}{\sigma_M} + \frac{\beta}{\sqrt{3}}\delta_{ij}, \tag{2.20}$$

$$s_{ij}^2 = \frac{3}{2}\frac{\sigma_{ij}^D}{\sigma_M} + \frac{\mu}{\sqrt{3}}\delta_{ij}. \tag{2.21}$$

It can readily be checked that eqn (2.17) reduces to the form (2.19) with s_{ij}^1, s_{ij}^2 given by eqns (2.20) and (2.21) if only we write out eqns (2.17) and (2.18) and define the parameters ζ, β and μ as

$$\bar{\zeta} = \zeta \frac{\omega + f\Sigma s}{(1 - f)\omega} - \frac{(c - f)\sigma_M}{\sigma\omega}\left[3f(1 - f)s + 2\frac{\hat{K}}{\sigma_M}\zeta\frac{\omega + f\Sigma s}{1 - f}\right], \tag{2.22}$$

$$\beta = \frac{\sqrt{3}}{2} \frac{fs}{\sqrt{\omega}},$$ (2.23)

$$\mu = \beta + \frac{(c+f)\hat{K}}{\sqrt{(3\omega)}}.$$ (2.24)

Here

$$\omega = 1 + f^2 - 2fc$$ (2.25)

is the square of the ratio of the macroscopic to microscopic equivalent yield strength

$$\omega = \frac{\bar{\sigma}^2}{\sigma_M^2}$$ (2.26)

and we have used the shortened notations

$$\Sigma \equiv \frac{\sigma_{kk}}{2\sigma_M}, \; s = \sinh \Sigma, \; c = \cosh \Sigma.$$ (2.27)

The standard derivation gives the constitutive relation of the non-associated plastic flow in the form analogous to (2.6) and (2.7) as

$$\dot{\sigma}_{ij} = L_{ijkl} d_{kl},$$ (2.28)

$$L_{ijkl} = L_{ijkl}^{(e)} - \bar{\alpha} \frac{\bar{s}_{ij}^1 \bar{s}_{ij}^2}{\bar{\zeta}^*} - \frac{1}{2}(\sigma_{ik} \delta_{jl} + \sigma_{jk} \delta_{il} + \sigma_{il} \delta_{jk} + \sigma_{jl} \delta_{ik}),$$ (2.29)

$$\bar{s}_{ij}^1 = L_{ijkl}^{(e)} s_{kl}^1 = \sqrt{3} \left(G \frac{\sqrt{3} \sigma_{ij}^D}{\sigma_M} + \mu K \delta_{ij} \right),$$ (2.30)

$$\bar{s}_{ij}^2 = L_{ijkl}^{(e)} s_{kl}^2 = \sqrt{3} \left(G \frac{\sqrt{3} \sigma_{ij}^D}{\sigma_M} + \beta K \delta_{ij} \right).$$ (2.31)

$$\bar{\zeta}^* = \zeta^* + \bar{s}_{ij}^1 s_{ij}^2 = \zeta + 3G + 3\beta\mu K,$$ (2.32)

or, more explicitly, eqn (2.7)

$$L_{ijkl} = \frac{E}{1+\nu} \left[\frac{\nu}{1-2\nu} \delta_{ij} \delta_{kl} + \frac{1}{2}(\delta_{ik} \delta_{jl} + \delta_{il} \delta_{jk}) \right]$$

$$- \bar{\alpha} \frac{\left(G \frac{\sqrt{3} \sigma_{ij}^D}{\sigma_M} + K_\beta \delta_{ij} \right) \left(G \frac{\sqrt{3} \sigma_{kl}^D}{\sigma_M} + K_\mu \delta_{kl} \right)}{\frac{1}{3}\zeta + G + \mu\beta K} - \frac{1}{2}(\sigma_{ik} \delta_{jl} + \sigma_{jk} \delta_{il} + \sigma_{il} \delta_{jk} + \sigma_{jl} \delta_{ik})$$

$$= \left(K - \frac{2}{3} G \right) \delta_{ij} \delta_{kl} + G (\delta_{ik} \delta_{jl} + \delta_{il} \delta_{jk})$$

$$- \frac{\left(G \frac{\sqrt{3} \sigma_{ij}^D}{\sigma_M} + K_\beta \delta_{ij} \right) \left(G \frac{\sqrt{3} \sigma_{ij}^D}{\sigma_M} + K_\mu \delta_{kl} \right)}{\frac{1}{3}\zeta + G + \mu\beta K} - \frac{1}{2}(\sigma_{ik} \delta_{jl} + \sigma_{jk} \delta_{il} + \sigma_{il} \delta_{jk} + \sigma_{jl} \delta_{ik}).$$ (2.33)

The condition for continued plastic deformation is now [24]

$$\frac{1}{\zeta} \left[\frac{\sigma_{ij}^D}{\sigma_M} + \frac{\mu}{\sqrt{3}} \delta_{ij} \right] \dot{\sigma} \geq 0.$$ (2.34)

Dealing with the J_2-flow theory we have obtained two expressions for the plastic strain rate. Equation (2.1) of the J_2-theory is seen to be a counterpart of eqn (2.19) of the Gurson's theory. The counterpart of eqn (2.13) is now, clearly, eqn (2.29) and eqn (90) of[25]

$$d_{ij}^{(p)} = s_{ij}^1 \frac{s_{kl}^2 L_{klmn}^{(e)} d_{mn}}{\zeta^* + s_{kl}^1 L_{klmn}^{(e)} s_{mn}^2} = s_{ij}^1 \frac{s_{kl}^2 \dot{\sigma}_{kl}}{\zeta + 3G + 3\mu\beta K}. \tag{2.35}$$

3. SOLUTION ALGORITHM

All the numerical results discussed below have been obtained by means of the finite element computer system LARSTRAN at the Institute of Statics and Dynamics, University of Stuttgart. The simple TRIAX 3 axisymmetric finite elements have been exclusively used; in the course of many numerical experiments they were found sufficiently accurate in modelling the problem under consideration, at least for the discretization mesh shown in Fig. 1 and used for all the computations. The numerical algorithm is described below. For the sake of presentation clarity the subsequent short discussion is confined to geometrically linear problems. However, it remains to replace in the algorithm the elastic stiffness matrix $K_{\alpha\beta}^{(e)}$ by the sum $K_{\alpha\beta}^{(e)} + K_{\alpha\beta}^{(\sigma)}$, the
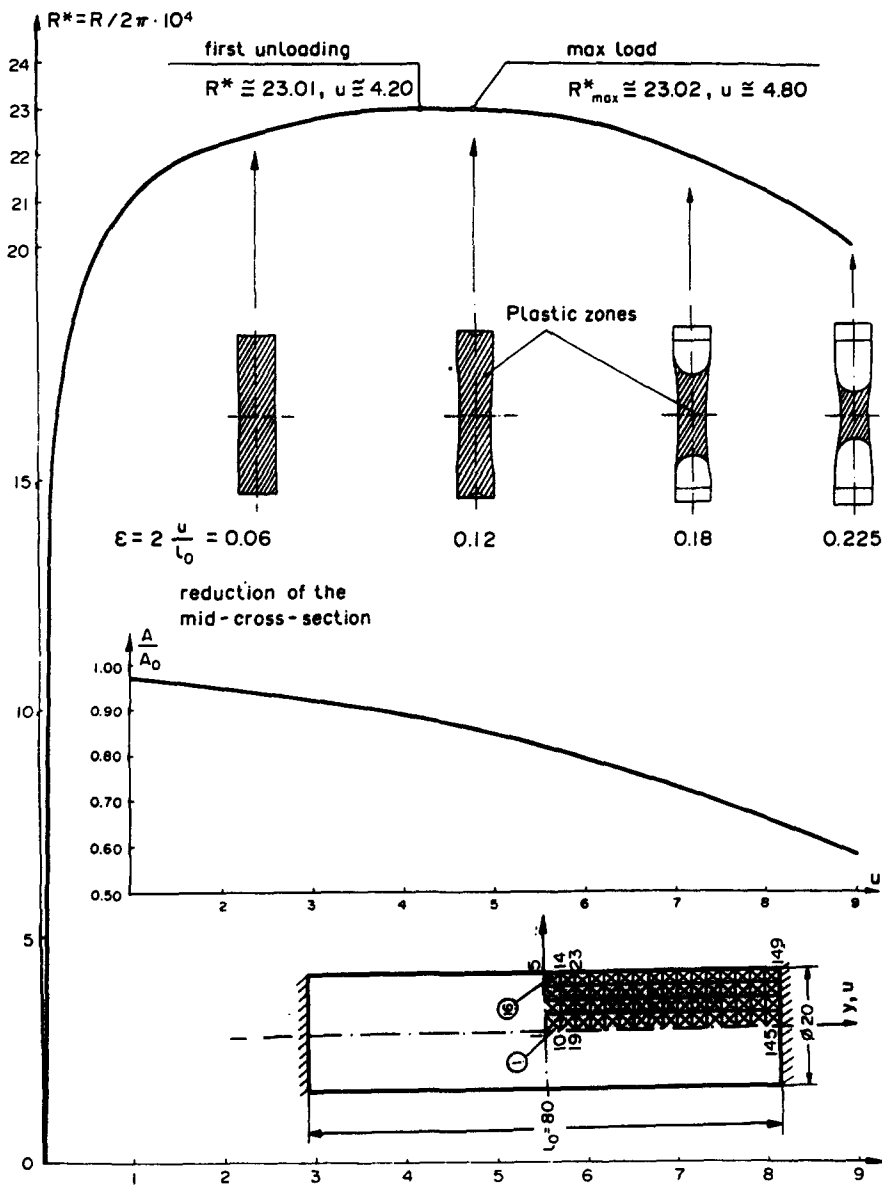

Fig. 1. Necking of a cylindrical specimen with built-in ends—J_2-flow theory.

second term being the initial stress matrix, and to remember about appropriate geometry updating and stress transformations, and the large deformation formulation is immediately recovered.

The numerical algorithm will be described in terms of finite increments of particular functions rather than in terms of their rates. Moreover, the quasi-static character of the analysis allows the time-like parameter t to be identified with any one-parameter controlled set of variables specific to the problem under consideration. In the case to be discussed these are the y-displacements at nodal points 145–149, Fig. 1.

Let us write out the fundamental matrix equation of equilibrium as, eqn (2.29)

$$(K^{(e)}_{\alpha\beta} + {}^-K^{(p)}_{\alpha\beta}) \Delta r_\beta = \Delta R_\alpha + {}^-R_\alpha - {}^-F_\alpha, \quad \alpha, \ \beta = 1, 2, \ldots, N \tag{3.1}$$

where

$$K^{(e)}_{\alpha\beta} = \sum_{\text{elem.}} \int_{V_{\text{elem.}}} B_{ij\alpha} \, B_{kl\beta} \, L^{(e)}_{ijkl} \, \mathrm{d}V, \tag{3.2}$$

$$ {}^-K^{(p)}_{\alpha\beta} = - \sum_{\text{elem.}} \int_{V_{\text{elem.}}} B_{ij\alpha} \, B_{kl\beta} \, \frac{\bar{s}^1_{ij} \, \bar{s}^2_{kl}}{\bar{\zeta}^*} \, \mathrm{d}V. \tag{3.3}$$

${}^-R_\alpha$ = vector of nodal external loads at the beginning of the current step, ΔR_α = vector of load increments at the current step; Δr_α = vector of nodal displacement increments; ${}^-F_\alpha$ = vector of internal nodal forces equivalent to the element stresses at the beginning of the step;

$$ {}^-F_\alpha = \sum_{\text{elem.}} \int_{V_{\text{elem.}}} B_{ij\alpha} \, {}^-\sigma_{ij} \, \mathrm{d}V, \tag{3.4}$$

N = total number of degrees of freedom, and the geometric matrix $B_{ij\alpha}$ is defined as

$$\Delta \epsilon_{ij} = d_{ij} \, \Delta t = B_{ij}\alpha \, \Delta r_\alpha \tag{3.5}$$

$\Delta \epsilon_{ij}$ being the incremental strain. The vector ${}^-R_\alpha - {}^-F_\alpha$ is called the unequilibrated nodal force vector at the beginning of the step. The labels "–" and "+" will further be used referring to values of functions at the beginning at the end of the time step considered.

It is important to realize that in nonlinear analysis eqn (3.1) represents a linear approximation to the actual system behaviour in each time step. Depending on the nonlinearities in the system and the magnitude of the time step Δt, the linearization may introduce severe drift-away errors and, in some cases, solution instability. Therefore, eqn (3.1) should be in general augmented by an iterative procedure. This is a crucial factor in evaluating all the existing computational algorithms leading ultimately to either the initial load or Newton–Raphson formulations. To discuss this issue more closely we rewrite eqn (3.1) as

$$K^{(e)}_{\alpha\beta}\Delta r_\beta = \Delta R_\alpha + {}^-R_\alpha - {}^-F_\alpha - {}^-K^{(p)}_{\alpha\beta}\Delta r_\beta. \tag{3.6}$$

This form of the equilibrium equation suggests clearly an iteration scheme to be used for its solution; to see this it is enough to rewrite eqn (3.6) as

$$K^{(e)}_{\alpha\beta} \, \Delta r_\beta^{(k)} = \Delta R_\alpha + {}^-R_\alpha - {}^-F_\alpha - {}^-K^{(p)}_{\alpha\beta}\Delta r_\beta^{(k-1)} \tag{3.7}$$

or, denoting

$$J_\alpha^{(p)(k-1)} = {}^-K^{(p)}_{\alpha\beta} \, \Delta r_\beta^{(k-1)} \tag{3.8}$$

as

$$K^{(e)}_{\alpha\beta} \, \Delta r_\beta^{(k)} = \Delta R_\alpha + {}^-R_\alpha - {}^-F_\alpha - J_\alpha^{(p)(k-1)}. \tag{3.9}$$

In fact the initial load term $J_\alpha^{(p)(k-1)}$ can be easier accounted for in the computer program if we represent it as

$$J_\alpha^{(p)(k-1)} = -\sum_{\text{elem.}} \int_{V_{\text{elem.}}} B_{ij\alpha} L_{ijkl}^{(e)} \Delta\epsilon_{kl}^{(p)(k-1)} \, dV \tag{3.10}$$

where

$$\Delta\epsilon_{ij}^{(p)} = d_{ij}^{(p)} \Delta t \tag{3.11}$$

is the incremental plastic strain. Now, this strain can be computed within the iteration loop according to the relations (2.19) or (2.35); the initial strain and initial stress schemes are then recovered, respectively. Equations (2.19) and (2.35) are most effectively utilized if we transform them to the form [25]

$$\Delta\epsilon_{ij}^{(p)(k)} = {}^+s_{ij}^{(k)} \left(\frac{{}^+\bar\sigma^{(k)} - {}^-\bar\sigma}{{}^-\zeta} + \sqrt{3}{}^-\mu \, \frac{{}^+\sigma_H^{(k)} - {}^-\sigma_H}{{}^-\zeta} \right) \tag{3.12}$$

$$\Delta\epsilon_{ij}^{(p)(k)} = {}^+s_{ij}^{(k)} \, \frac{{}^+\bar\sigma^{*(k)} - {}^-\bar\sigma}{{}^-\zeta + 3G\left(1 + {}^-\beta{}^-\mu \frac{K}{G}\right)} + \sqrt{3}{}^-\mu \, \frac{{}^+\sigma_H^{*(k)} - {}^-\sigma_H}{{}^-\zeta + 3G\left(1 + {}^-\beta{}^-\mu \frac{K}{G}\right)} \tag{3.13}$$

where

$$\sigma_H = \frac{1}{3}\sigma_{kk} \tag{3.14}$$

is the hydrostatic pressure,

$$ {}^+\bar\sigma^{(k)} = \left(\frac{3}{2}{}^+\sigma_{ij}^{D(k)} {}^+\sigma_{ij}^{D(k)}\right)^{1/2}. \tag{3.15}$$

$$ {}^+\bar\sigma^{*(k)} = \left[\frac{3}{2}({}^-\sigma_{ij}^D + \Delta\sigma_{ij}^{D*(k)})({}^-\sigma_{ij}^D + \Delta\sigma_{ij}^{D*(k)}). \tag{3.16}$$

Expressions (3.12) and (3.13) are formed on the basis of the state at the beginning of the step; the analogous expressions based upon continuously updated reference state need not be recalled. It should also be noted that in deriving eqns (3.12) and (3.13) some terms have been assumed negligible to[25]. The residual vector after mth iteration is defined as

$$R_{\alpha(\text{res})}^{(m)} = \Delta R_\alpha + {}^-R_\alpha - \Delta J_\alpha^{(p)(m)} - K_{\alpha\beta}^{(e)} \Delta r_\beta^{(m)} \tag{3.17}$$

upon which a convergence criterion can be imposed in the form

$$\frac{\|R_{\alpha(\text{res})}\|}{\|{}^+R_\alpha\|} \leqslant \text{``tolerance''} \tag{3.18}$$

for instance. If "m" is the number of the last iteration needed to satisfy the condition (3.18) then $R_{\alpha(\text{res})}^{(m)}$ is taken as the unequilibrated internal force vector for the next step, eqn (3.1).

Let us now pass to the short discussion of the Newton–Raphson iteration scheme. To this aim we rewrite original equilibrium equation (3.1) as

$$\hat K_{\alpha\beta}^{(k-1)} \delta r^{(k)} = {}^+R_\alpha - {}^-F_\alpha - \Delta J_\alpha^{(p)(k-1)} - \Delta J_\alpha^{(e)(k-1)} \tag{3.19}$$

where

$$\Delta J_\alpha^{(e)(k-1)} \equiv K_{\alpha\beta}^{(e)} \Delta r_\beta^{(k-1)}, \tag{3.20}$$

$\delta r_\alpha^{(k)} = k$th correction to the incremental displacements so that after kth iteration the kth approximation to the incremental displacement vector reads

$$\Delta r_\alpha^{(k)} = \sum_{i=1}^{k} \delta r_\alpha^{(i)}, \quad \delta r_\alpha^{(1)} \equiv \Delta r_\alpha, \quad \text{see eqn (3.1)}$$

while $\hat{K}_{\alpha\beta}$ is a stiffness matrix to be specified later. The vectors $^-F_\alpha$ and $\Delta J_\alpha^{(p)(k-1)}$ are defined by eqn (3.4) and eqn (3.10) while the vector $\Delta J_\alpha^{(e)(k-1)}$ is given by

$$\Delta J_\alpha^{(e)(k-1)} = \sum_{\text{elem.}} \int_{V_{\text{elem.}}} B_{ij\alpha}{}^+\sigma_{ij}^{*(k-1)} \, dV = \sum_{\text{elem.}} \int_{V_{\text{elem.}}} B_{ij\alpha} L_{ijkl}^{(e)} \Delta \epsilon_{kl}^{(k-1)} \, dV. \quad (3.21)$$

Equation (3.19) allows to define the current internal force vector as

$$^+F_\alpha^{(k-1)} = {}^-F_\alpha + \Delta J_\alpha^{(e)(k-1)} + \Delta J_\alpha^{(p)(k-1)} \quad (3.22)$$

which, on account of eqns (3.4), (3.10) and (3.21) becomes

$$^+F_\alpha^{(k-1)} = \sum_{\text{elem.}} \left\{ \int_{V_{\text{elem.}}} B_{ij\alpha} \left[{}^-\sigma_{ij} + L_{ijkl}^{(e)} (\Delta\epsilon_{kl}^{(k-1)} - \Delta\epsilon_{kl}^{(p)(k-1)}) \right] dV \right\} \quad (3.23)$$

$$= \sum_{\text{elem.}} \int_{V_{\text{elem.}}} B_{ij\alpha}{}^+\sigma_{ij}^{(k-1)} \, dV.$$

The equation describing the Newton–Raphson iteration takes the final form

$$\hat{K}_{\alpha\beta} \delta r_\beta^{(k)} = {}^+R_\alpha - {}^+F_\alpha^{(k-1)} \quad (3.24)$$

in which $^+F_\alpha^{(k-1)}$ is the vector of internal nodal point forces equivalent to the element stresses at the end of the step after the $(k-1)$th correction. The matrix $\hat{K}_{\alpha\beta}$ is formed in the program anew either at each iteration ("full" Newton–Raphson iteration) or at the beginning of the step only (modified Newton–Raphson iteration), according to the definition

$$\hat{K}_{\alpha\beta} = K_{\alpha\beta}^{(e)} + K_{\alpha\beta}^{(p)} \Big|_{\substack{\beta=0 \\ \mu=0}}. \quad (3.25)$$

This choice assures: (a) good convergence properties of the iteration even for advanced plastic flow and (b) no problems with the "non-symmetric" stiffness terms resulting from the existence of the parameters β and μ in the elastic–plastic constitutive equation. The effects of "non-symmetry" of the problem formulation are entirely accounted for at the stage of constructing the internal force vector $^+F_\alpha^{(k-1)}$, see eqn (3.23). Some other details of the numerical procedure are given in [25].

4. BOUNDS TO PRIMARY BIFURCATION STATE

Consider a hypoelastic solid obtained from the J_2-elastic–plastic solid by putting $\alpha = 1$, see eqn (2.7). This hypothetical solid is routinely referred to as the Hill's linear comparison solid, [1, 2]. It is well known [4], that the first eigenstate for this solid (i.e. such a state for which a non-trivial solution is possible for the associated homogeneous rate problem) may often be identified with some bifurcation state for the underlying elastic–plastic solid, since the actual bifurcation mode for the latter can be determined by forming an appropriate liner combination of the eigenmode and the fundamental solution. The Hill's theory of bifurcation has been recently generalized to include a non-associated flow law [26]. Two kinds of comparison solids have been proposed. The first is a one-parameter family of linear solids that admit a potential and have the property that if uniqueness (i.e. no bifurcation) is certain for the comparison solid then bifurcation is precluded for the underlying elastic–plastic solid. The bifurcation point

found for such a comparison solid gives in this way a lower bound to the ordinarily unknown magnitude of the primary bifurcation for the solid with non-associated flow rule (without potential).

The second comparison solid has been introduced in [26] in analogy to the Hill's "no unloading" solid and can be obtained from the genuine elastic–plastic solid by putting $\bar{\alpha} = 1$ in eqn (2.29). The first eigenstate of such a comparison solid gives an upper bound to the primary bifurcation state of the underlying elastic–plastic solid with non-associated flow rule.

The comparison solids are of great practical importance as they allow to replace the search for the genuine primary bifurcation by a search for upper and lower bounds corresponding to the bifurcation points in solids which are analytically more simple to describe.

Let us now have a closer look at the first kind of non-associated plasticity comparison solids. The one-parameter family of such fictitious solids is defined by the constitutive equation of the form

$$\dot{\bar{\sigma}}_{ij} = \hat{L}_{ijkl}\, d_{kl} \tag{4.1}$$

$$\hat{L}_{ijkl} = L^{(e)}_{ijkl} - \frac{1}{4r\zeta^*}(s^1_{ij} + rs^2_{ij})(s^1_{kl} + rs^2_{kl}) - \frac{1}{2}(\sigma_{ik}\delta_{jl} + \sigma_{jk}\delta_{il} + \delta_{il}\delta_{ik} + \sigma_{jl}\delta_{ik}) \tag{4.2}$$

where the scalar parameter r is assumed to be positive. As shown in [26], the basic practical meaning of this fictitious comparison solid rests upon the fact that bifurcation of an elastic–plastic body cannot precede primary bifurcation of the comparison body. Furthermore, the constitutive relation for the comparison body is not only linear but admits the potential which has the same structure as the corresponding potential for the elastic–plastic body obeying normality. It is also worthwhile to note that the tensor that specifies the direction of the plastic strain rate is for the comparison body replaced by $(s^1_{ij} + rs^2_{ij})/2\sqrt{r}$. Therefore, the methods of analysis of bifurcation (the appropriate computer programs, in particular) that have been developed so far for elastic–plastic solids obeying normality may now also be used to determine the lower bounds to bifurcation states in solids with a non-associated flow law. The questions of accuracy of such bounds and of the choice of the parameter r still remain to be answered. In general, however, the parameter r which can be a function of particle position should be optimized in every specific situation to give the bound closest, in some sense, the primary bifurcation state of the genuine solid.

In order to take into account in the computational procedure the comparison solid defined by eqns (4.1) and (4.2) we note that now

$$s_{ij} = \frac{1}{2\sqrt{r}}(s^1_{ij} + r\,s^2_{ij}) \tag{4.3}$$

and

$$d^{(p)}_{ij} = \frac{1}{\zeta}\, s_{ij}\,(s_{kl}\,\dot{\sigma}_{kl}) = \frac{3}{2}\frac{\sigma^D_{ij}}{\sigma_M}\frac{1+r}{2\sqrt{r}} + \frac{1}{3}\delta_{ij}\frac{\beta + r\mu}{2\sqrt{r}}. \tag{4.4}$$

It is readily seen that to obtain a code capable of dealing with the "symmetric" comparison solid from the program designed for the non-associated plasticity analysis it is enough to replace σ^D_{ij} by $\sigma^D_{ij}(1 + r/2\iota r)$ and β and μ by $(\beta + r\mu/2\sqrt{r})$. Carrying out the bifurcation analysis with such a modified program we obtain the results which should give a lower bound to the bifurcation state of the genuine solid.

Now, in order to get an upper bound to the primary bifurcation states in non-associated plasticity problems we simply use the hypoelastic solid defined by eqns (2.6) and (2.7) with $\bar{\alpha} = 1$ ("no unloading" comparison solid). The first eigenstate of this solid is the upper bound to the primary bifurcation state of the elastic–plastic solid. The numerical implementation of the constitutive equation for such comparison solids is straightforward as it suffices to merely exclude the unloading branch from the origninal formulation.

5. RESULTS AND DISCUSSION

The computational algorithm developed in the previous section has been implemented into the computer system LARSTRAN and used for a detailed study of the circular cylindrical bar

in uniaxial tension enforced by an axial displacement rate prescribed at the ends of the bar. The geometric data for the problem are given in Fig. 1; the material properties are: $E = 2.1 \cdot 10^6$, $\nu = 0.3$, $\sigma_0 = 2.0 \cdot 10^3$, Ramberg–Osgood hardening curve of the form $\bar{\epsilon}^{(p)} = (1.1 \sigma_0/mE)[(\sigma_M/1.1 \sigma_0)^M - (1/1.1)^m]$, $m = 8$. The uniform finite element idealization by means of 256 TRIAX 3 elements is also shown. In each calculation to be discussed below the overall elongation of 0.225 times the initial specimen length is imposed in 300 equal steps of prescribed displacements of the ends so that finally the engineering strain of $\epsilon_y^{max} = (300 \times 0.03/40) = 0.225$ is achieved. The boundary value problem is posed in two ways: in one the ends are assumed to be cemented to rigid grips, while in the other they remain shear free. A bifurcation from a state of uniform tensile stress occurs with the latter end-condition only. Nevertheless, we start with a short discussion of the results obtained for the bar with the built-in ends.

The specimen is first analysed within the framework of the flow theory. Curve of the resultant reaction R versus prescribed displacement u, the development of unloading zones with the increasing deformation and the gradual reduction of the cross-section area at neck are shown in Fig. 1. It is noted that in contrary to the results given in [6] the whole specimen goes
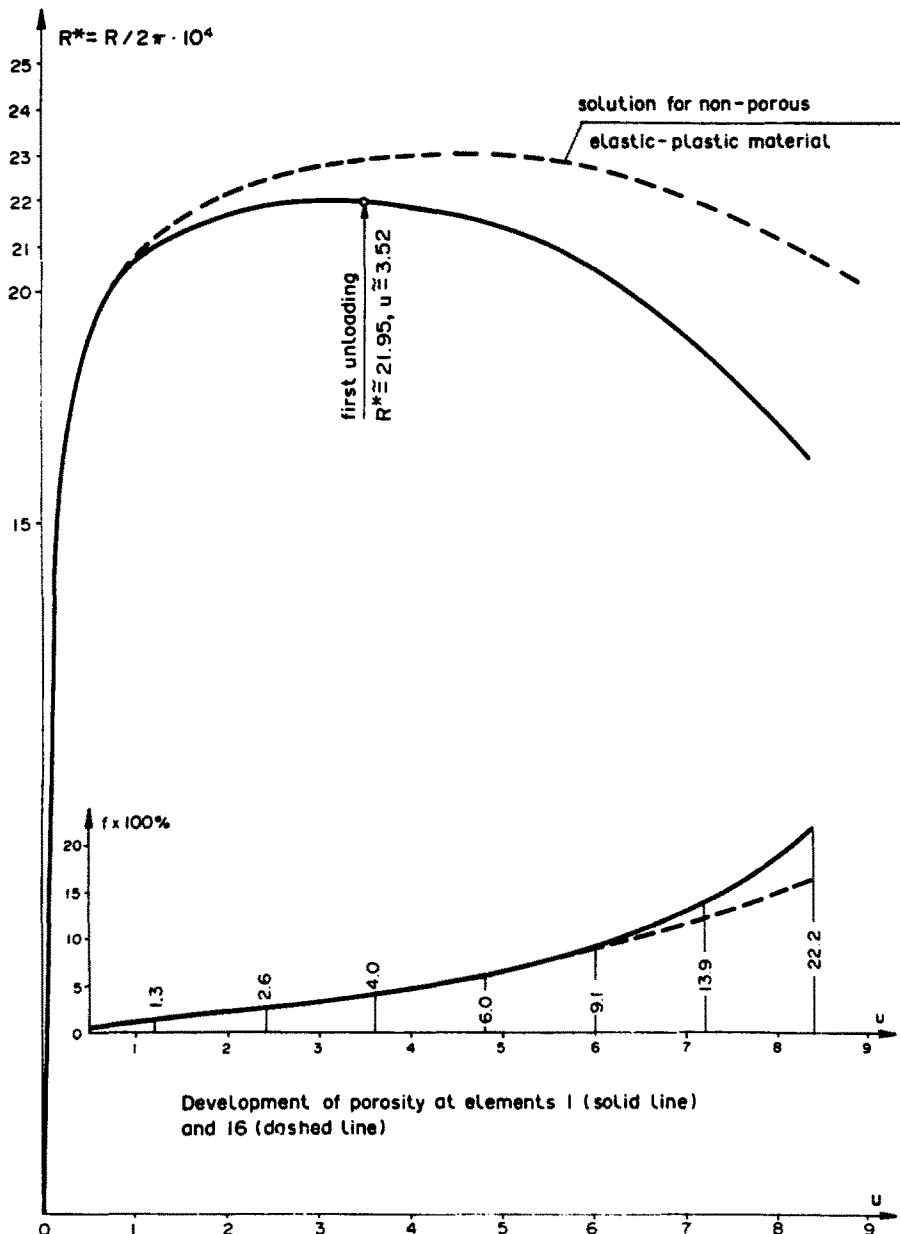
Fig. 2. Necking of a cylindrical specimen with built-in ends—Gurson's theory for $\dot{K} = 0.001$, $f_0 = 0.00$.

plastic before it starts to unload. In other words, no region remains elastic throughout the entire range of straining. Furthermore the unloading starts at distinctly smaller strains than those accompanying the maximum load point. As expected, no sudden change in the slope of the cross-section reduction curve is observed.

The calculations are next repeated for the porous material assuming $\hat{K} = 0.001$, eqn (2.16), and no initial voids in the material, $f_0 = 0.00$. The resultant reaction vs prescribed displacement curve obtained for such a material is compared against the previous curve in Fig. 2. The development of porosity in the neck at the element 1 (near the axis of the bar) and at element 16 (near the lateral surface of the bar), Fig. 1, are also shown.

The next example is that of the bar with shear-free ends analysed within the framework of the J_2-flow theory, Fig. 3. The curve $C\emptyset$ corresponds to the bar with perfect geometry while the curve $C1$ is obtained by assuming an initial mid-cross-section reduction of 0.5%. The first
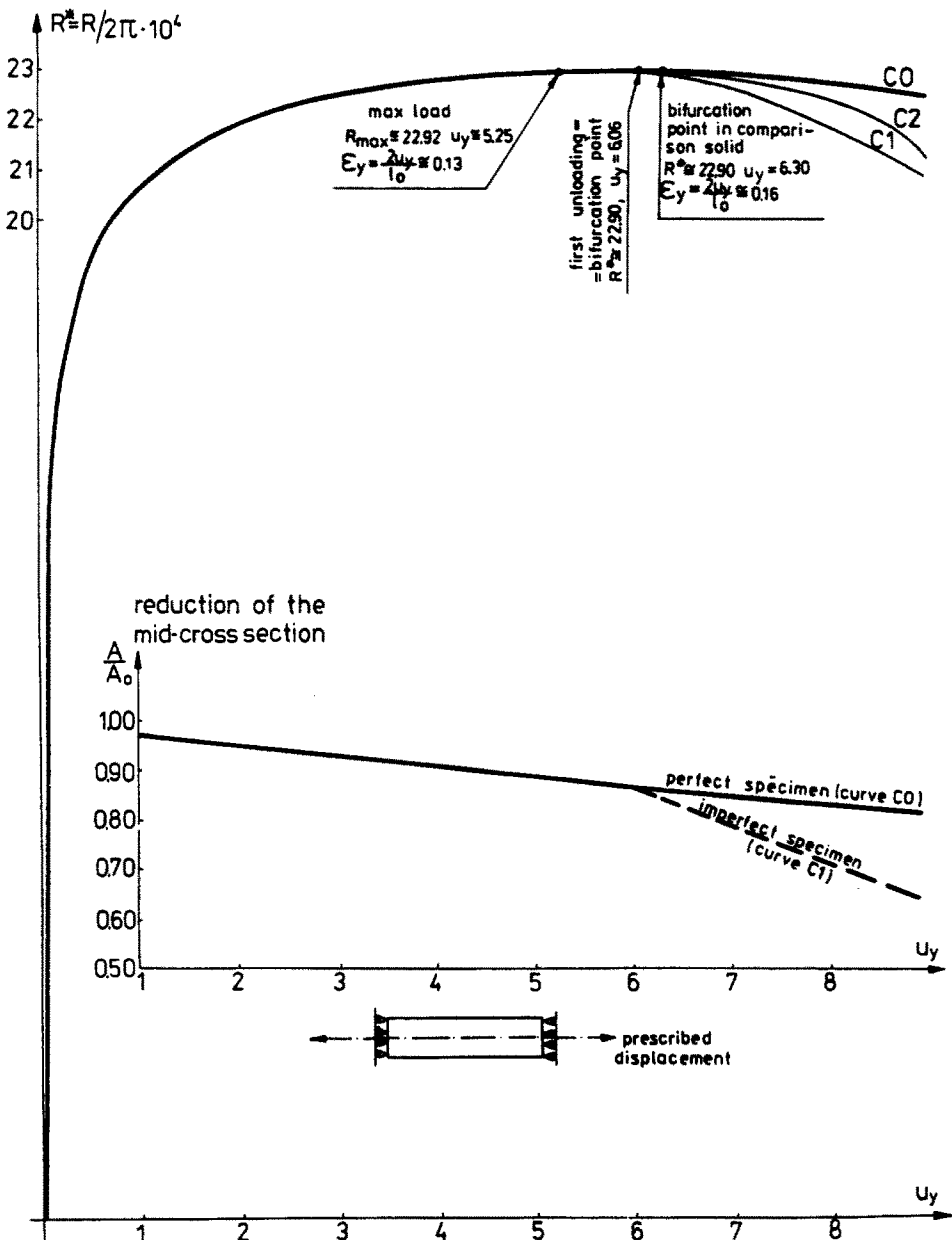
Fig. 3. Necking of a cylindrical specimen with simply supported (shear free) ends—J_2-flow theory and the corresponding Hill's comparison solid (no unloading).

unloading point on the curve $C1$ is clearly identified as the primary bifurcation point for the J_2-elastic–plastic material. At about the same deformation the area of the neck starts to decrease much more rapidly as compared against the perfect geometry specimen.

Now, the calculation for the bar with the slight geometric imperfection is repeated assuming the Hill's "no unloading" comparison solid. On the so-obtained characteristic curve $C2$ the bifurcation point is approximately identified. In accordance with the properties of the J_2-elastic–plastic material this point should coincide with the bifurcation point in the genuine elastic–plastic material, but this is confirmed by the present numerical calculations only approximately. However, it should be stressed that the way the branching point is effectively identified may contribute significantly to its final location along the equilibrium curve. In particular, the bifurcation point for the comparison solid in this case owes its location to the fact that the solution for the "no unloading" solid follows closely the fundamental curve $C0$ in the post-bifurcation range of deformation which makes a clear distinction of this point difficult. In the present approach it is done by assuming an *a priori* threshold value of $0.001 \cdot R^*$ for the difference between the normalized reactions of both the fundamental and imperfect solutions. With all these reservations the imperfection-type approach to the bifurcational problems via the comparison solid concept seems to yield an interesting information as the effective inclusion of the unloading criterion in some numerical analyses can turn out troublesome.

The distribution of stresses at neck for two different stages of the process in the J_2-material are shown in Fig. 4 (for the perfect specimen—the fundamental solution) and in Fig. 5 (for the imperfect specimen). It is seen that the peak stresses in the latter case are on the axis of the bar
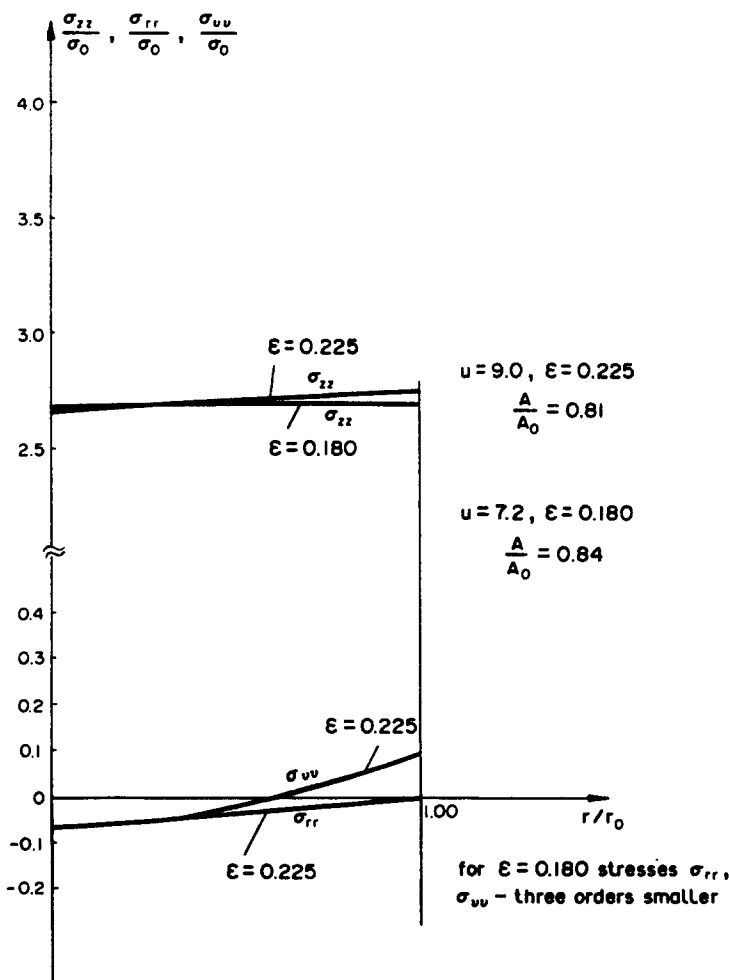

Fig. 4. Stress distribution at mid-cross-section for $\epsilon = 0.180$ and $\epsilon = 0.225$, perfect non-porous elastic-plastic specimen (curve $C0$, Fig. 3).
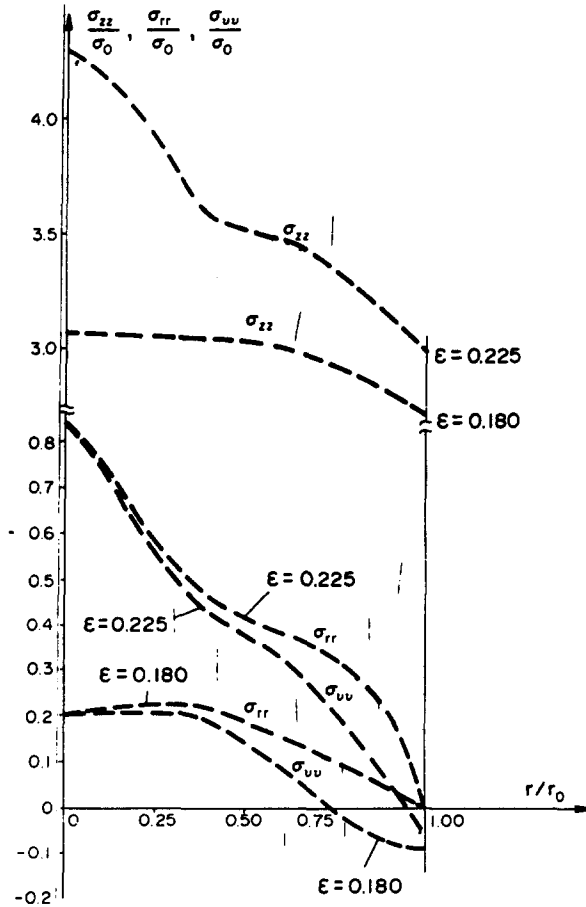
Fig. 5. Stress distribution at mid-cross-section for $\epsilon = 0.180$ and $\epsilon = 0.225$, imperfect non-porous elastic-plastic specimen (curve C1, Fig. 3).

which confirms the results of [6] and contradicts those given in [13]. The peaks become accentuated as necking proceeds. The two next comparisons, Figs. 6 and 7, are made for equivalent and hydrostatic stresses at neck. This is followed by the equivalent plastic strain distribution shown in Fig. 8.

Now, we pass to a detailed analysis of the necking process in the porous elastic–plastic material. All the analyses are carried out for specimens with the perfect geometric shape and the shear-free ends. Imperfections are introduced into the problem by assuming the existence of initial, non-uniform void distributions. The following notation is used in Fig. 9:

C0—fundamental solution for the J_2-flow theory without voids,

C1—fundamental solution for elastic–plastic void-containing material imperfections,

C2—solution for elastic–plastic void-containing material, $\hat{K} = 0.001$, initial porosity $f_0 = 0.01$ at elements 1–16, Fig. 1,

C3—solution for elastic–plastic void-containing comparison material, ("no unloading"), $\hat{K} = 0.001$, initial porosity $f_0 = 0.01$ at elements 1–16,
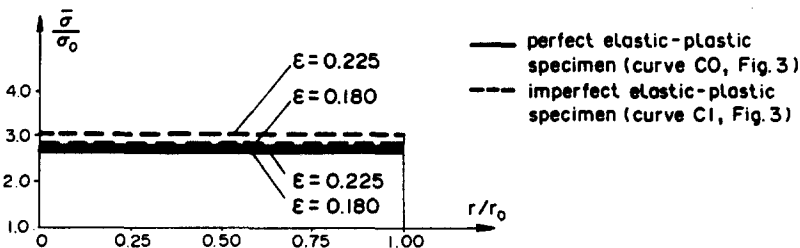

Fig. 6. Equivalent stress distribution at mid-cross-section for $\epsilon = 0.180$ and $\epsilon = 0.225$, perfect and imperfect non-porous elastic–plastic specimen.
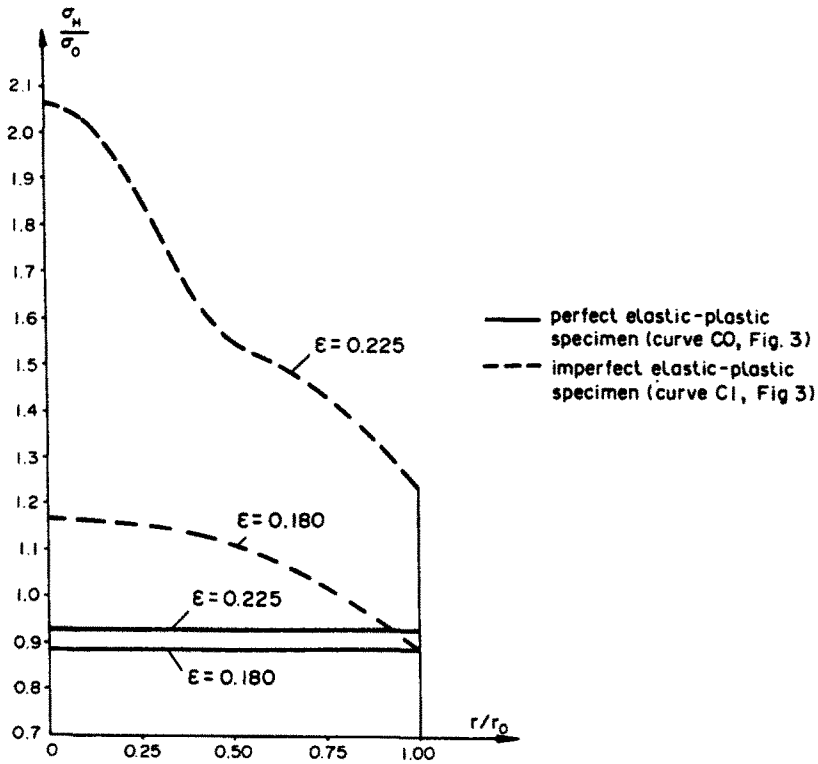
Fig. 7. Hydrostatic stress distribution at mid-cross-section for $\epsilon = 0.180$ and $\epsilon = 0.225$, perfect and imperfect non-porous elastic–plastic specimen.
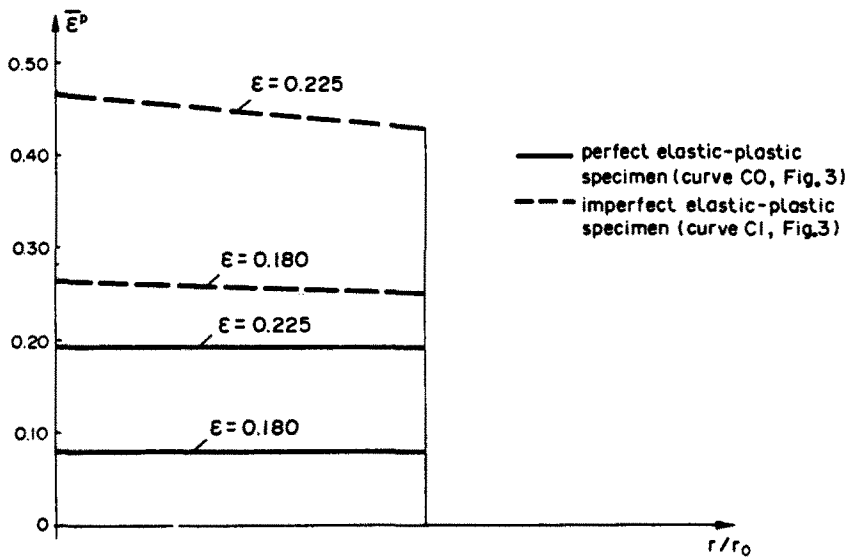

Fig. 8. Equivalent plastic strain distribution at mid-cross-section for $\epsilon = 0.180$ and $\epsilon = 0.225$, perfect and imperfect non-porous elastic–plastic specimen.

$C4$—solution for elastic–plastic void-containing comparison material ("symmetric", $r = 1$), $\hat{K} = 0.001$, initial porosity at elements 1–16. This solution has been obtained by carrying out the calculations for the genuine void-containing material and testing for branching at subsequent equilibrium points by solving each time additionally the incremental problem with the "symmetric" comparison solid and assuming a threshold value for the difference in the incremental solutions,

B_2, B_3, B_4—conjectural bifurcation points for problems characterized by the curves $C2$, $C3$, $C4$,
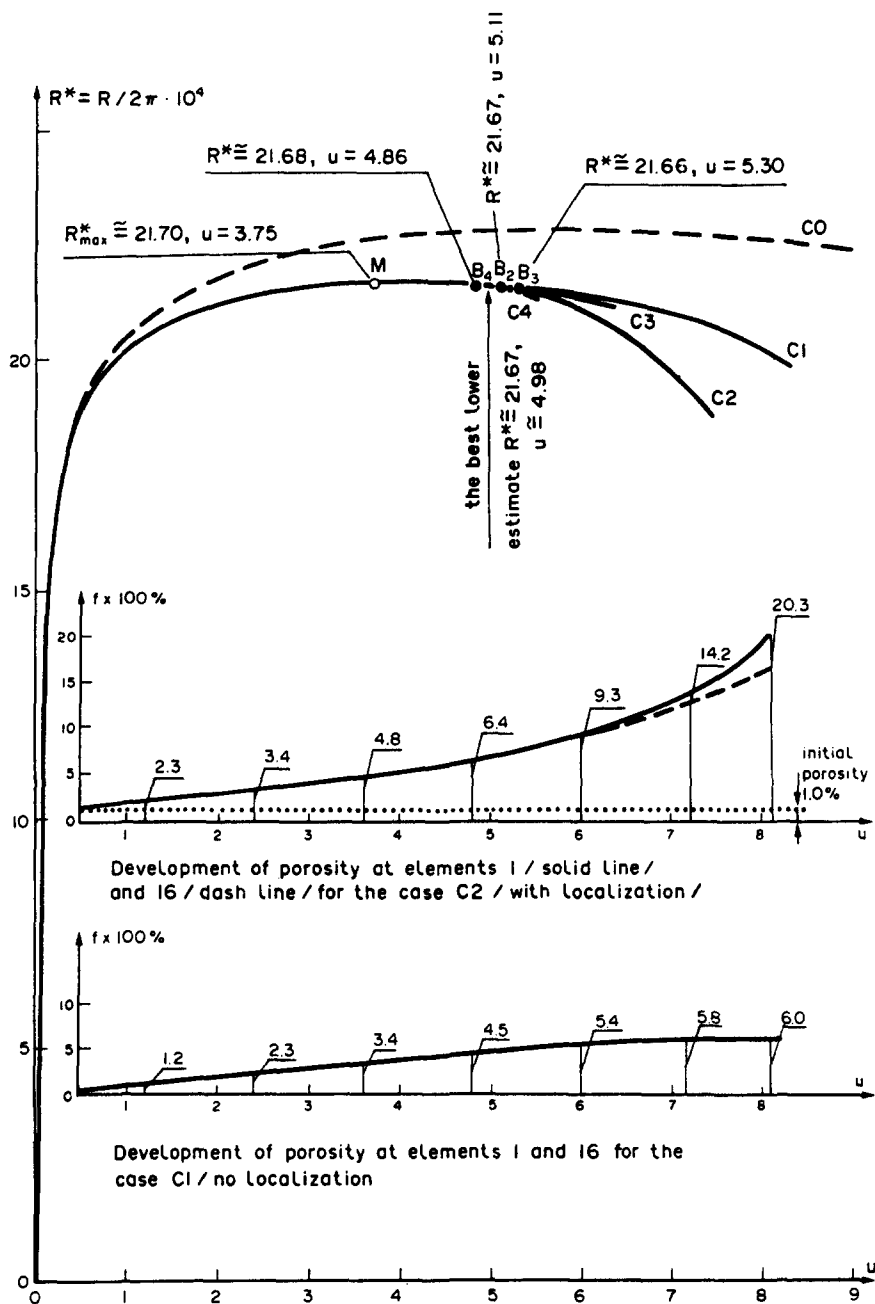
M—maximum load point.

Fig. 9. Necking of a cylindrical specimen with simply supported (shear free) ends—Gurson's theory and the corresponding comparison solids.

It is seen from Fig. 9 that the development of the deformation process for the porous bar is essentially similar to that observed in the non-porous bar. The piont B_2 is identified as the point at which unloading begins. At about the same point the sudden change in the slope of the cross-section reduction curve is clearly visible, Fig. 10. The significant increase in porosity is seen in Fig. 9 for the case of the localized plastic flow; no such effect accompanies the non-localized solution.

The points B_4 and B_3 are obtained on the basis of the Raniecki's comparison solids. As it is clearly seen from Fig. 9 the bounding analyses give very good estimates to the primary bifurcation point in the genuine porous material. The optimization of the lower bound is discussed later. The subsequent figures deal with the neck distribution of stress components,
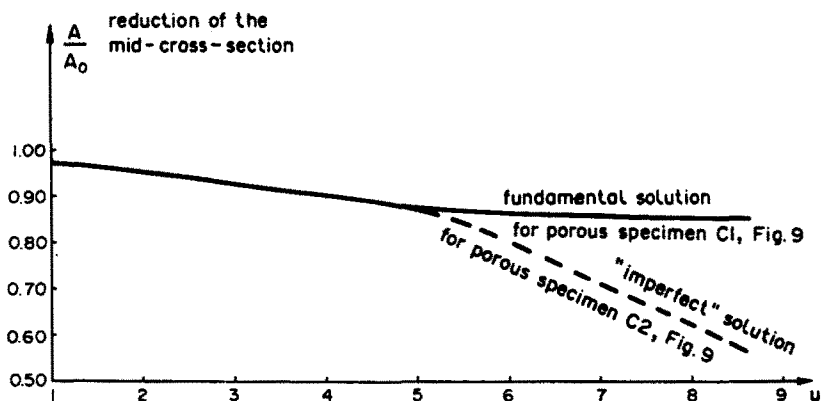
Fig. 10. Reduction of the mid-cross-section for the imperfect porous specimen (curve C2, Fig. 9).

Fig. 11, equivalent stress Fig. 12, hydrostatic stress, Fig. 13, equivalent plastic strain, Fig. 14 and porosity, for both perfect and imperfect porous elastic–plastic specimens.

As we pointed out in Section 4, the closeness of the lower estimate to the primary bifurcation point depends very strongly upon the choice of the parameter r entering the constitutive equation for the comparison solid. A number of test calculations has been carried out each time with different value of the parameter r; r was assumed constant throughout the
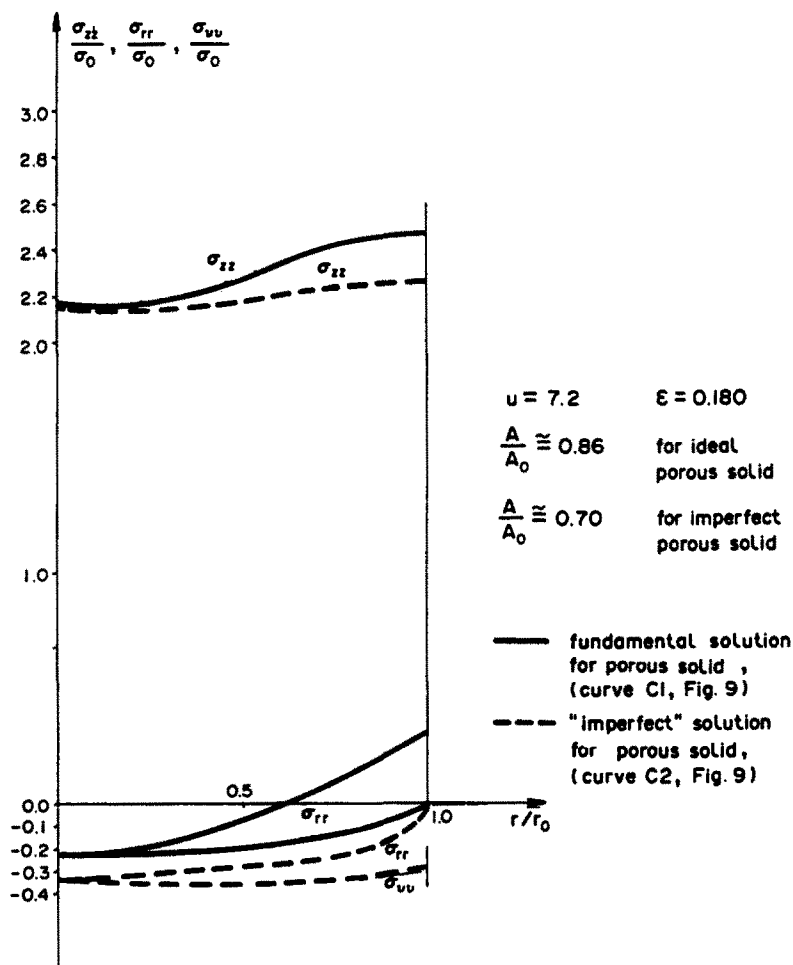

Fig. 11. Stress disribution at mid-cross-section fro $\epsilon = 0.180$, perfect and imperfect porous elastic–plastic specimen.
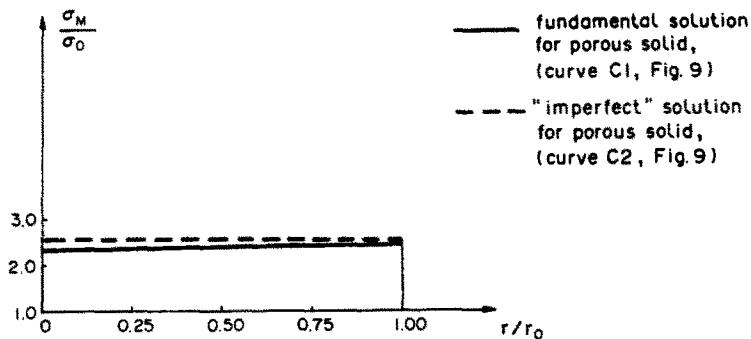
M. KLEIBER

Fig. 12. Equivalent stress distribution at mid-cross-section for $\epsilon = 0.180$, perfect and imperfect porous elastic–plastic specimen.
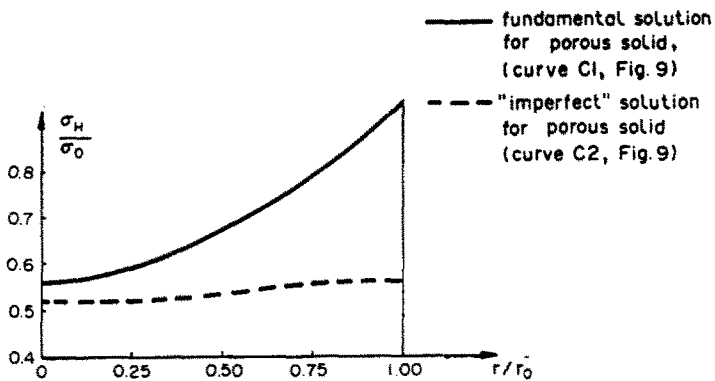

Fig. 13. Hydrostatic stress distribution at mid-cross-section for $\epsilon = 180$, perfect and imperfect porous elastic–plastic specimen.
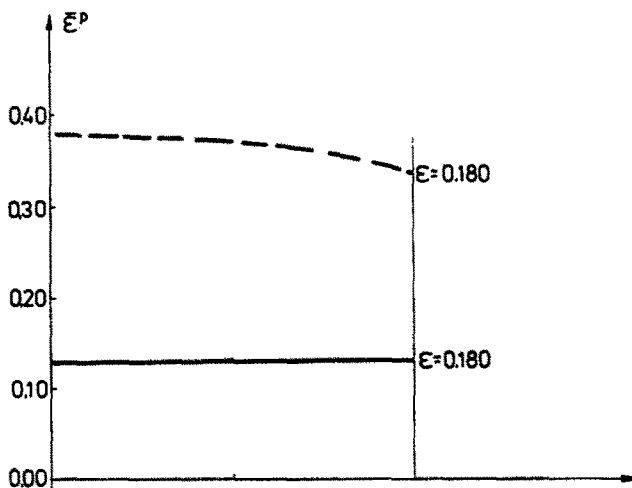

Fig. 14. Equivalent plastic strain distribution at mid-cross-section for $\epsilon = 0.180$, perfect and imperfect porous elastic–plastic specimen.
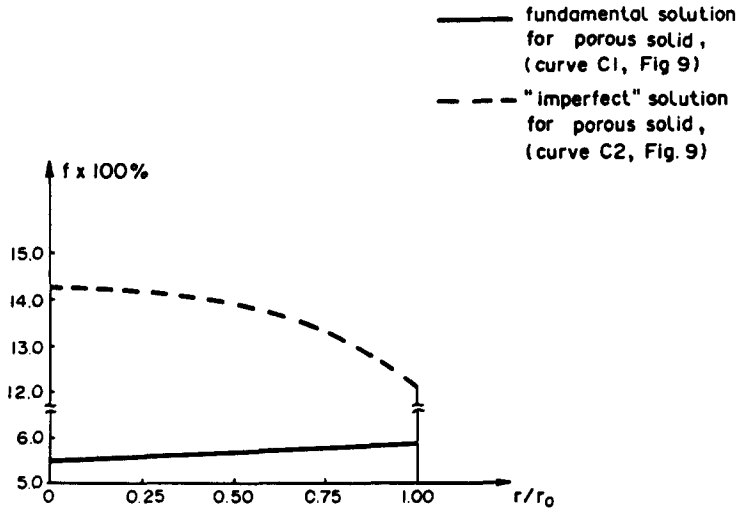
Fig. 15. Porosity distribution at mid-cross-section for $\epsilon = 0.180$, perfect and imperfect porous elastic-plastic specimen.

whole plastic region, though. The displacements at the bifurcation for different values of r are shown in Fig. 16. It is seen that the best lower bound is given by the "symmetric" comparison solid with $r = 0.9$.

6. CONCLUSIONS

(1) Analysis of the bifurcation phenomenon by means of the direct integration approach known in classical plasticity has also turned out operative for void-containing materials.

(2) The Gurson's theory applied to the axisymmetric necking of the porous specimen seems to yield results which are qualitatively reliable.

(3) The finite element incremental approach combined with the Newton–Raphson iteration and the consequent definitions of the initial strain expressions seems to be very well suited for the analysis of large deformation non-associated plasticity problems.

(4) The concept of the linear comparison solids introduced recently for the analysis of non-associated plastic flow seems to offer a very effective tool for obtaining reliable lower and upper bounds to the primary bifurcation states.

Detailed analysis of the sensitivity of the bifurcation predictions to the material and geometry imperfections is postponed to a forthcoming paper.
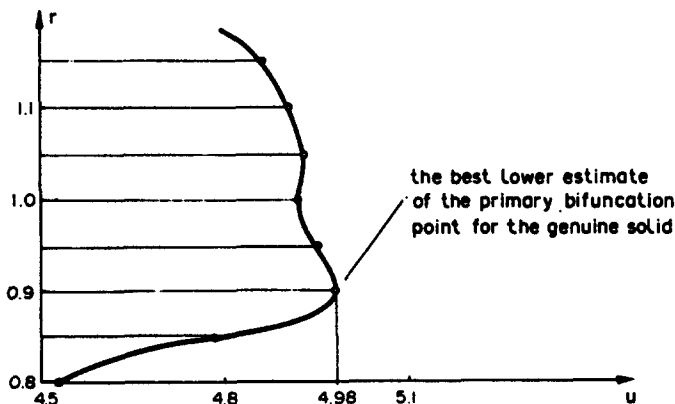

Fig. 16. Influence of the parameter r on the estimation of the bifurcation point by means of the "symmetric" comparison solid.

REFERENCES

1. R. Hill, A general theory of uniqueness and stability in elastic–plastic solids. *J. Mech. Phys. Sol.* **6**, 236–249 (1958).
2. R. Hill, Bifurcation and uniqueness in nonlinear mechanics of continua. *Problems of Continuum Mechanics*, pp. 155–164. S.I.A.M. Philadelphia (1961).
3. J. P. Miles, Bifurcation in plastic flow under uniaxial tension. *J. Mech. Phys. Sol.* **19**, 89–102 (1971).
4. J. W. Hutchinson and J. P. Miles, Bifurcation analysis of the onset of necking in an elastic–plastic cylinder under uniaxial tension. *J. Mech. Phys. Sol.* **22**, 61–79 (1974).
5. S. Y. Cheng, S. T. Ariaratnam and R. N. Dubey, Axisymmetric bifurcation in an elastic–plastic cylinder under axial load and lateral hydrostatic pressure. *Quart. Appl. Math.* **29**, 41–51 (1971).
6. A. Needleman, A numerical study of necking in circular cylindrical bars. *J. Mech. Phys. Sol.* **20**, 111–127 (1972).
7. A. Needleman and V. Tvergaard, Necking of biaxially stretched elastic–plastic circular plates. *J. Mech. Phys. Sol.* **25**, 159–183 (1977).
8. V. Tvergaard, Bifurcation and imperfection—sensitivity at necking instabilities. *ZAMM* **60**, T26–T34 (1980).
9. J. W. Hutchinson, Plastic buckling. *Advances in Applied Mechanics* (Edited by C. S. Yih), Vol. 14, pp. 67–144 (1974).
10. J. W. Hutchinson, Imperfection sensitivity in the plastic range. *J. Mech. Phys. Sol.* **21**, 191–204 (1973).
11. V. Tvergaard, Buckling behaviour of plate and shell structures. *Proc. 14th Cong. Theor. Appl. Mech.* (Edited by W. T. Koiter), pp. 233–247 (1976).
12. J. R. Osias and J. L. Swedlow, Finite elasto–plastic deformation—I. Theory and numerical examples. *Int. J. Solids. Structures* **10**, 321–340 (1974).
13. W. H. Chen, Necking of a bar. *Int. J. Solids. Structures* **7**, 685–717 (1971).
14. R. M. McMeeking and J. R. Rice, Finite element formulations for problems of large elastic–plastic deformation. *Int. J. Solids Structures* **11**, 601–616 (1975).
15. J. H. Argyris and M. Kleiber, Incremental, discretized formulation in non-linear mechanics and finite strain elasto-plasticity—natural approach, Part I. *Comp. Meths. Appl. Mech. Engng* **11**, 215–247 (1977).
16. M. Kleiber, J. A. König and A. Sawczuk, Studies on plastic structures: stability, cyclic loadings, anisotropic hardening. *Proc. FENOMECH 81, University of Stuttgart*, also: *Comp. Meths. Appl. Mech. Engng* (1982).
17. J. W. Hutchinson, Finite strain analysis of elastic–plastic solids and structures. *Num. Sol. Nonlinear Struct. Problems* (Edited by R. F. Hartung) ASME, 17.
18. Z. Mróz, On forms of constitutive laws for elastic–plastic solids. *Arch. Mech. Stos.* **18**, 3–35 (1966).
19. A. L. Gurson, Continuum theory of ductile rupture by void nucleation and growth—I. Yield criteria and flow rules for porous ductile media. *J. Engng Materials Tech.* **99**, 2–15 (1977).
20. A. L. Gurson, Porous rigid-plastic materials containing rigid inclusions—yield function, plastic potential, and void nucleation. *Proc. Int. Conf. Fracture* (Edited by D. M. R. Taplin), Vol. 2A, pp. 357–364 (1977).
21. H. Yamamoto, Conditions for shear localization in the ductile fracture of void-containing materials. *Int. J. Fract.* **14**, 347–365 (1978).
22. A. Needleman and J. R. Rice, Limits to ductility set by plastic flow localization. *Mech. Sheet Metal Forming* (Edited by D. P. Koistinen and N.-M. Wang) pp. 237–266 (1978).
23. C.-C. Chu and A. Needleman, Void nucleation effects in biaxially stretched sheets. MRL E118, Brown University (1979).
24. V. Tvergaard, On localization in ductile materials containing spherical voids. *Int. J. Fracture* **18**, 237–252 (1982).
25. J. H. Argyris and M. Kleiber, Finite elements in non-associated plasticity—axisymmetric necking in void-containing materials. *Comp. Meths. Appl. Mech. Engng* (1982).
26. B. Raniecki and O. T. Bruhns, Bounds to bifurcation stresses in solids with non-associated plastic flow law at finite strain. *J. Mech. Phys. Solids* **29**, 153–172 (1982).